Structural Engineering and Mechanics, Vol. 8, No. 6 (1999) 591-605
DOI: http://dx.doi.org/10.12989/sem.1999.8.6.591

An accurate and efficient shell element with improved reduced integration rules

Z.H. Zhong†

College of Mechanical and Automotive Engineering, Hunan University, Changsha, China

M.J. Tan‡ and G.Y. Li‡†

School of Mechanical and Production Engineering, Nanyang Technological University, Nanyang Avenue, Singapore 639798

Abstract. An accurate and efficient shell element is presented. The stiffness of the shell element is decomposed into two parts with one part corresponding to stretching and bending deformation and the other part corresponding to shear deformation of the shell. Both parts of the stiffness are calculated with reduced integration rules, thereby improving computational efficiency. Shear strains are averaged on the reference surface such that neither locking phenomena nor any zero energy mode can occur. The satisfactory behaviour of the element is demonstrated in several numerical examples.

Key words : shell element; locking; zero energy modes; cross reduced integration.

1. Introduction

Over the last two decades, extensive research work has been devoted to the developments of shell element with great achievements (Belytschko 1981 to Zienkiewicz 1977). Despite that fact, further developments on this area are still desirable. A common numerical deficiency encountered in shell finite elements is the transverse shear locking phenomenon. The locking phenomenon becomes more and more pronounced as the thickness of the element becomes smaller and smaller. An efficient way to overcome the locking phenomenon is to use reduced integration rules to calculate the element stiffness matrix as discussed in literatures (Zienkiewicz 1977, Hughes 1987, Cook 1981, and Zienkiewicz 1971). Reduced integration rules are also used to improve computational efficiency. While reduced integration rules do solve the locking problem and improve computational efficiency, they may cause numerical disasters, i.e., zero-energy modes or hourglass modes. To cope with zero-energy modes introduced by the reduced integration technique, a lot of researches have been done. For instance, in earlier papers, Belytschko *et al.* (1981, 1983, 1984) and Liu *et al.* (1985) have developed reduced integration shell elements by embedding the hourglass control. The main process of hourglass control has been constructed by

† Professor
‡ Associate Professor
‡† Research Fellow

introducing parameters for artificial damping and artificial stiffness. Recently, Belytschko and co-workers (1994) developed a 4-node quadrilateral reduced integration shell element. An assumed strain method was used to stabilize the zero energy modes. Vu-Quoc (1989) developed a series of rank one perturbations on the stiffness matrix to filter the spurious zero energy modes. In Vu-Quoc (1990), this method was intended for dynamic analysis. The method consisted of a perturbation of the under integrated stiffness matrix to fully compensate its rank and a projection of the mass matrix to nullify the generalized mass of some spurious modes. In this paper, efforts are made to introduce new reduced integration rules which solve the locking problem and improve computational efficiency but does not introduce any zero-energy mode. This integration technique is based on the cross reduced integration technique described by Zhong (1991). The element integration carried out in this paper is, however, different from that in Zhong (1991). In the following, the element stiffness will be decomposed into two parts. The first part is associated with the stretching and bending deformation and is integrated along the central fiber of the element. The second part is associated with the shear deformation and is integrated both on the reference surface and the central fiber of the element. Shear strains on the reference surface are averaged such that neither the locking phenomenon nor any zero energy mode can occur.

2. Shell element formulation

2.1. General formulation

The shell element formulation is based on the well-known definition of laminas and fibers, and will basically follow the procedures as described by Hughes (1987). Only four-node bilinear shell elements are considered. Small displacements and elastic materials are assumed for the elements. Since the shell element formulation is standard and is well known, some details will be skipped in the following. For further details of the shell formulation, readers are refered to Hughes (1987).

In this shell formulation, two local coordinate systems are used. These two coordinate systems are the so-called fiber coordinate system and lamina coordinate system. The base vectors in a fiber coordinate system are denoted by v_1, v_2 and v_3. The base vectors in a lamina coordinate system are denoted by e_1, e_2 and e_3 as shown in Fig. 1.

The geometry of the element at any deformed state can be defined as follows:

$$t_X = \sum_{k=1}^{4} N_k(\xi, \eta) t_x^k + \frac{1}{2}\zeta \sum_{k=1}^{4} N_k(\xi, \eta)\, h^k t_{v_3}^k \tag{1}$$

where t_X denotes the position vector of a point in the shell element, t_x^k the nodal value of t_X, (ξ, η, ζ) the isoparametric coordinates of a point in the element, h^k the thickness at node k, $N_k(\xi, \eta)$ the shape function associated with node k, and $t_{v_3}^k$ an unit vector at node k in the fiber direction.

The displacement field within the shell element can then be obtained as follows:

$$u = \sum_{k=1}^{4} N_k(\xi, \eta) u^k + \frac{1}{2}\zeta \sum_{k=1}^{4} N_k(\xi, \eta) h^k w^k \tag{2}$$

where u^k is the displacement of node k, and w^k is the change of the base vector along the fiber. Assuming small displacements, we can approximate w^k as

$$w^k = -\theta_1^k v_2^k + \theta_2^k v_1^k \tag{3}$$

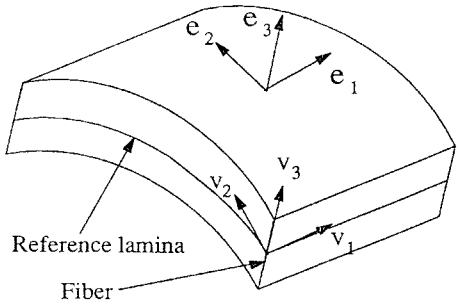

Fig. 1 A shell element with lamina and fiber

where θ_1^k and θ_2^k are the rotations of the fiber around v_1^k and v_2^k respectively.

The geometry and the displacement in the lamina coordinate system can be obtained as

$$x_i^1 = \sum_{k=1}^{3} Q_{ik} x_k \tag{4}$$

$$u_i^1 = \sum_{k=1}^{3} Q_{ik} u_k \tag{5}$$

where u_i^1 denotes the displacement component in the lamina coordinate system, and Q_{ik} the transformation matrix defined as follows:

$$Q = [e_1\, e_2\, e_3]^T \tag{6}$$

2.2. Strain-displacement matrix

Define two strain vectors $\varepsilon_\varepsilon^1$ and ε_γ^1 in the lamina coordinate system and displacement vector d as follows:

$$\varepsilon_\varepsilon^1 = [\varepsilon_{11}^1, \varepsilon_{22}^1]^T \tag{7}$$

$$\varepsilon_\gamma^1 = [2\varepsilon_{12}^1, 2\varepsilon_{23}^1, 2\varepsilon_{31}^1]^T \tag{8}$$

$$d = [\cdots u_1^k, u_2^k, u_3^k, \theta_1^k, \theta_2^k, \cdots]^T \tag{9}$$

where ε_{33}^1 is omitted because its associated normal stress component is conventionally assumed zero, and

$$\varepsilon_{ij}^1 = \frac{1}{2}\left(\frac{\partial u_i^1}{\partial x_j^1} + \frac{\partial u_j^1}{\partial x_i^1}\right) \tag{10}$$

From Eqs. (2) to (10), it can be found that

$$\varepsilon_\varepsilon^1 = B_\varepsilon d \tag{11}$$

$$\varepsilon_\gamma^1 = B_\gamma d \tag{12}$$

where B_ε and B_γ are strain - displacement matrices calculated as follows:

$$B_\varepsilon = \begin{bmatrix} Z_{1,1} \\ Z_{1,2} \end{bmatrix} H_{\xi\eta} \tag{13}$$

$$B_\gamma = \begin{bmatrix} Z_{1,2}+Z_{2,1} \\ Z_{2,3}+Z_{3,2} \\ Z_{3,1}+Z_{1,3} \end{bmatrix} H_{\xi\eta} \tag{14}$$

where

$$Z_{ij} = [Q_{i1}\Gamma^1_{j1}, Q_{i1}\Gamma^1_{j2}, Q_{i1}\Gamma^1_{j3}, Q_{i2}\Gamma^1_{j1}, Q_{i2}\Gamma^1_{j2}, Q_{i2}\Gamma^1_{j3}, Q_{i3}\Gamma^1_{j1}, Q_{i3}\Gamma^1_{j2}, Q_{i3}\Gamma^1_{j3}] \tag{15}$$

$$H_{\xi\eta} = \begin{bmatrix} H_{1,\xi} \\ H_{1,\eta} \\ H_{1,\zeta} \\ \vdots \\ H_{3,\zeta} \end{bmatrix} \tag{16}$$

$$H_1 = [N_1, 0, 0, -0.5\zeta N_1 h^1 v_{21}, 0.5\zeta N_1 h^1 v_{11}, \cdots] \tag{17}$$

$$H_2 = [0, N_1, 0, -0.5\zeta N_1 h^1 v_{22}, 0.5\zeta N_1 h^1 v_{12}, \cdots] \tag{18}$$

$$H_3 = [0, 0, N_1, -0.5\zeta N_1 h^1 v_{23}, 0.5\zeta N_1 h^1 v_{13}, \cdots] \tag{19}$$

where Γ^1_{jk} denotes an element in the inverse of the Jacobin matrix in the lamina coordinate system.

2.3. Element stiffness matrix and reduced integration rules

The element stiffness matrix is then given by the standard finite element formulation, i.e.,

$$K = \int_{\Omega^e} B_\varepsilon^T C_\varepsilon B_\varepsilon dV + \int_{\Omega^e} B_\gamma^T C_\gamma B_\gamma dV = K_\varepsilon + K_\gamma \tag{20}$$

where

$$K_\varepsilon = \int_{\Omega^e} B_\varepsilon^T C_\varepsilon B_\varepsilon dV \tag{21}$$

$$K_\gamma = \int_{\Omega^e} B_\gamma^T C_\gamma B_\gamma dV \tag{22}$$

$$C_\varepsilon = \frac{E}{(1-\nu^2)} \begin{bmatrix} 1 & \nu \\ \nu & 1 \end{bmatrix} \tag{23}$$

$$C_\gamma = \frac{E}{(1-\nu^2)} \begin{bmatrix} (1-\nu)/2 & 0 & 0 \\ 0 & \kappa(1-\nu)/2 & 0 \\ 0 & 0 & \kappa(1-\nu)/2 \end{bmatrix} \tag{24}$$

where κ is a shear correction factor and κ=5/6.

To improve computational efficiency, the first part of stiffness K_ε is now integrated with a reduced integration rule $1\times1\times(2n+1)$, $n\geq0$, which means a reduced integration along the central fiber with $2n+1$ integration points. Thus, we have

$$K_\varepsilon = 4\sum_{i=1}^{2n+1}(B_\varepsilon^T C_\varepsilon B_\varepsilon J)_{\xi_0\,\eta_0\,\zeta_i} W_{\zeta_i} \tag{25}$$

where $(*)_{\xi_0\,\eta_0\,\zeta_i}$ indicates that the expression in the parenthesis is evaluated at (ξ_0, η_0, ζ_i) and ξ_0= η_0=0.

To evaluate the second part of the stiffness K_γ, we use a cross reduced integration rule as described in Zhong (1991). Thus, the strain-displacement matrix is partitioned as follows:

$$B_\gamma = B_{\gamma1} + B_{\gamma2} \tag{26}$$

where

$$B_{\gamma1} = \begin{bmatrix} Z_{1,2}+Z_{2,1} \\ Z_{2,3}+Z_{3,2} \\ Z_{3,1}+Z_{1,3} \end{bmatrix} H^u_{\xi\eta} \tag{27}$$

$$B_{\gamma2} = \begin{bmatrix} Z_{1,2}+Z_{2,1} \\ Z_{2,3}+Z_{3,2} \\ Z_{3,1}+Z_{1,3} \end{bmatrix} H^\theta_{\xi\eta} \tag{28}$$

$$H^u_{\xi\eta} = \begin{bmatrix} H_{1u,\xi} \\ H_{1u,\eta} \\ H_{1u,\zeta} \\ \vdots \\ H_{3u,\zeta} \end{bmatrix} \tag{29}$$

$$H^\theta_{\xi\eta} = \begin{bmatrix} H_{1\theta,\xi} \\ H_{1\theta,\eta} \\ H_{1\theta,\zeta} \\ \vdots \\ H_{3\theta,\zeta} \end{bmatrix} \tag{30}$$

where

$$H_{1u} = [N_1, 0, 0, 0, 0, \cdots] \tag{31}$$

$$H_{2u} = [0, N_1, 0, 0, 0, \cdots] \tag{32}$$

$$H_{3u} = [0, 0, N_1, 0, 0, \cdots] \tag{33}$$

$$H_{1\theta} = [0, 0, 0, -0.5\zeta N_1 h^1 v_{21}, 0.5\zeta N_1 h^1 v_{11}, \cdots] \tag{34}$$

$$H_{2\theta} = [0, 0, 0, -0.5\zeta N_1 h^1 v_{22}, 0.5\zeta N_1 h^1 v_{12}, \cdots] \tag{35}$$

$$H_{3\theta} = [0, 0, 0, -0.5\zeta N_1 h^1 v_{23}, 0.5\zeta N_1 h^1 v_{13}, \cdots] \tag{36}$$

By using the Gauss quadrature, Eq. (22) can be written as

$$K_\gamma = \sum_{i=1}^{m} \left(\int_\xi \int_\eta B_\gamma^T C_\gamma B_\gamma d\xi d\eta \right)_{\zeta_i} W_{\zeta_i} \tag{37}$$

where m denotes the total number of Gauss points in the fiber direction and is chosen to be $(2n+1)$, i.e., $m=2n+1$, in our study.

Thus, Eq. (37) can be written as

$$K_\gamma = \left(\int\int B_\gamma^T C_\gamma J d\xi d\eta \right)_{\zeta_0} W_{\zeta_0} + \sum_{i=1}^{2n} \left(\int\int B_\gamma^T C_\gamma B_\gamma J d\zeta d\eta \right)_{\zeta_i} W_{\zeta_i} \tag{38}$$

where W_{ζ_0} denotes the weigh at ζ and $\zeta_0=0$.

Now the first integration in Eq. (38) is calculated by using a 2×2 Gauss quadrature and the second by using a 1×1 Gauss quadrature, i.e.,

$$K_\gamma = \sum_{i=1}^{4} (B_\gamma^T C_\gamma B_\gamma J)_i W_{\zeta_0} + 4 \sum_{i=1}^{2n} (B_\gamma^T C_\gamma B_\gamma J)_{\xi_0 \eta_0 \zeta_i} W_{\zeta_i} \tag{39}$$

where $(*)_i$ indicates that the quantity $*$ is evaluated at integration point i on the reference lamina as shown in Fig. 2.

In the cross reduced integration technique, the partition of the B_γ matrix in Eqs. (26) to (36) is made use of and Eq. (39) is replaced by the following equation:

$$K_\gamma = \sum_{i=1}^{4} (\bar{B}^T)_i C_\gamma (\bar{B})_i (J)_i W_{\zeta_0} + 4 \sum_{i=1}^{2n} (B_\gamma^T C_\gamma B_\gamma J)_{\xi_0 \eta_0 \zeta_i} W_{\zeta_i} \tag{40}$$

where

$$(\bar{B})_1 = [\alpha (B_{\gamma 1})_1 + (B_{\gamma 1})_3]/(1+\alpha) + [(B_{\gamma 2})_1 + (B_{\gamma 2})_3]/2 \tag{41}$$

$$(\bar{B})_2 = [\alpha (B_{\gamma 1})_2 + (B_{\gamma 1})_4]/(1+\alpha) + [(B_{\gamma 2})_2 + (B_{\gamma 2})_4]/2 \tag{42}$$

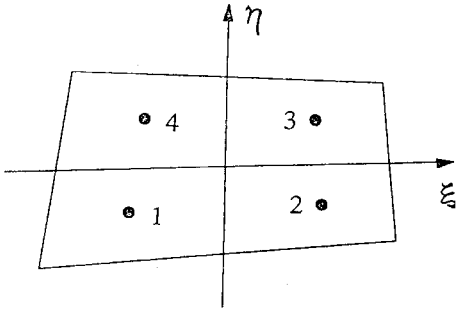

Fig. 2 Gauss points on the reference lamina

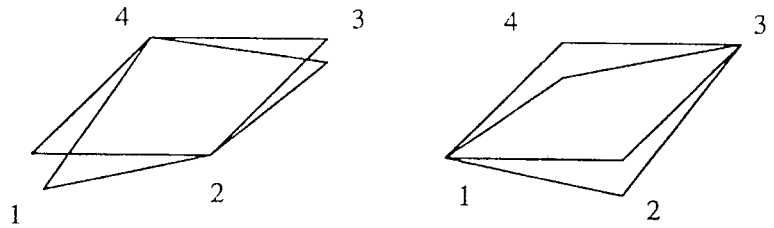

Fig. 3 Two possible zero energy modes of the shell element

$$\overline{(B)}_3 = [\alpha(B_{\gamma 1})_3 + (B_{\gamma 1})_1]/(1+\alpha) + [(B_{\gamma 2})_3 + (B_{\gamma 2})_1]/2 \tag{43}$$

$$\overline{(B)}_4 = [\alpha(B_{\gamma 1})_4 + (B_{\gamma 1})_2]/(1+\alpha) + [(B_{\gamma 2})_4 + (B_{\gamma 2})_2]/2 \tag{44}$$

In Eqs. (41) to (44), the parameter α may be considered as a weigh and the shear strains due to the translational degrees of freedom at integration points 1 and 3 and integration points 2 and 4 are thus averaged with the weight α. If α=1, K_γ calculated in Eq. (40) will have rank deficiency, producing two possible zero energy modes as shown in Fig. 3. By setting $\alpha > 1$, these two zero energy modes can be removed. Numerical experiences show that it is sufficient to set $\alpha \geq 1.01$ to eliminate those two zero energy modes. If α is too big, the element may be too stiff. Suggested values for α are between 1.05 and 1.20.

Another important consequence of the operations in Eqs. (41) to (44) is that the spurious shear strains due to the rotational degrees of freedom at point 1 and point 3 are averaged and so are the spurious shear strains at point 2 and point 4. By averaging the spurious shear strains at integration points 1 and 3 and integration points 2 and 4, the shear strains at these points due to pure bending cancels each other, thus solving the locking problem. At the same time, no zero energy mode associated with rotational degrees of freedom is possible. Furthermore, no zero energy mode associated with translational degrees of freedom is possible. Due to the fact that ζ=0 on the reference lamina, the computation work increased by integration on the reference lamina is not so significant as it would seemingly be the case. Since the total integration points in this reduced integration technique is in general more than that in the uniform reduced integration along the central fiber, stresses can be calculated at more locations, requiring more computation work and more storage space for stress calculation. On the other hand, however, no special zero energy control algorithm is required. Furthermore, using more integration points (without increasing too much computational work) can be an advantage from an accuracy point of view, especially for material nonlinearity analysis.

3. Numerical examples

To demonstrate the behavior of the shell element, some numerical examples are presented in the following. There are two main purposes in selecting these examples. First of all, the accuracy of the shell element is to be examined. Secondly, the capability of the element to resist zero energy modes is to be demonstrated.

3.1. Patch tests

The mesh layout which is used in the patch test is shown in Fig. 4. Two loading cases have

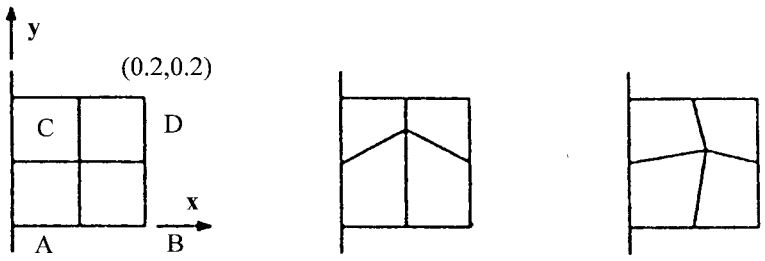

Fig. 4 Mesh layout for patch test: (a) regular mesh; (b) the first distorted mesh; (c) the last distorted mesh Young's modulus $E=10^{10}$ psi and Poisson's ratio $\nu=0.0$

Table 1 Stresses along the central fibre in the patch test for $\alpha=1.0$

$x=$	0.100	0.100	0.105	0.110	0.120
$y=$	0.100	0.1500	0.105	0.110	0.120
Element 1					
5	0.6462E+06	0.6462E+06	0.6466E+06	0.6478E+06	0.6478E+06
6	-0.6462E+06	-0.6462E+06	-0.6466E+06	-0.6478E+06	-0.6478E+06
7	0.1087E+07	0.1087E+07	0.1088E+07	0.1090E+07	0.1090E+07
8	-0.1087E+07	-0.1087E+07	-0.1088E+07	-0.1090E+07	-0.1090E+07
Element 2					
5	0.6462E+06	0.6462E+06	0.6466E+06	0.6426E+06	0.6274E+06
6	-0.6462E+06	-0.6462E+06	-0.6466E+06	-0.6426E+06	-0.6274E+06
7	0.1087E+07	0.1087E+07	0.1088E+07	0.1081E+07	0.1056E+07
8	-0.1087E+07	-0.1087E+07	-0.1088E+07	-0.1081E+07	-0.1056E+07
Element 3					
5	0.6462E+06	0.6462E+06	0.6466E+06	0.6401E+06	0.6162E+06
6	-0.6462E+06	-0.6462E+06	-0.6466E+06	-0.6401E+06	-0.6162E+06
7	0.1087E+07	0.1087E+07	0.1087E+07	0.1077E+07	0.1037E+07
8	-0.1087E+07	-0.1087E+07	-0.1087E+07	-0.1077E+07	-0.1037E+07
Element 4					
5	0.6462E+06	0.6462E+06	0.6462E+06	0.6512E+06	0.6664E+06
6	-0.6462E+06	-0.6462E+06	-0.6462E+06	-0.6512E+06	-0.6664E+06
7	0.1087E+07	0.1087E+07	0.1087E+07	0.1096E+07	0.1118E+07
8	-0.1087E+07	-0.1087E+07	-0.1087E+07	-0.1096E+07	-0.1118E+07

been considered. First, a uniformly line-distributed moment is applied along line BD. Different coordinates have been assigned to the middle node to get different distortion of the mesh as shown in Fig. 4. Furthermore, the parameter α is varied to check its effects on patch test. The results of the tests are shown in Table 1 for $\alpha=1.0$ and Table 2 for $\alpha=1.1$. In Table 1 and Table 2, number 5, 6, 7, 8 refer to Gauss points along the central fiber with ζ equal to ζ_a, $+\zeta_a$, $-\zeta_b$, $+\zeta_b$, respectively, where $\zeta_a < \zeta_b$. We can see that the stress distribution corresponds exactly to a constant bending deformation for the regular mesh and the first distorted mesh. The coordinates of the central node in the first distorted mesh are (0.1, 0.15). For other distorted meshes. The stress distribution deviates slightly (from 0.4 to 7 percent) from that due to a constant bending deformation. The parameter α has little effect on the results. In all the cases, the nodal forces

Table 2 Stresses along the central fibre in the patch test for α=1.1

x=	0.100	0.100	0.105	0.110	0.120
y=	0.100	0.1500	0.105	0.110	0.120
Element 1					
5	0.6462E+06	0.6461E+06	0.6464E+06	0.6472E+06	0.6460E+06
6	-0.6462E+06	-0.6461E+06	-0.6464E+06	-0.6472E+06	-0.6460E+06
7	0.1087E+07	0.1087E+07	0.1088E+07	0.1089E+07	0.1087E+07
8	-0.1087E+07	-0.1087E+07	-0.1088E+07	-0.1089E+07	-0.1087E+07
Element 2					
5	0.6462E+06	0.6461E+06	0.6451E+06	0.6419E+06	0.6256E+06
6	-0.6462E+06	-0.6461E+06	-0.6451E+06	-0.6419E+06	-0.6256E+06
7	0.1087E+07	0.1087E+07	0.1087E+07	0.1080E+07	0.1053E+07
8	-0.1087E+07	-0.1087E+07	-0.1087E+07	-0.1080E+07	-0.1053E+07
Element 3					
5	0.6462E+06	0.6461E+06	0.6446E+06	0.6398E+06	0.6157E+06
6	-0.6462E+06	-0.6461E+06	-0.6446E+06	-0.6398E+06	-0.6157E+06
7	0.1087E+07	0.1087E+07	0.1085E+07	0.1077E+07	0.1036E+07
8	-0.1087E+07	-0.1087E+07	-0.1085E+07	-0.1077E+07	-0.1036E+07
Element 4					
5	0.6462E+06	0.6461E+06	0.6471E+06	0.6502E+06	0.6611E+06
6	-0.6462E+06	-0.6461E+06	-0.6471E+06	-0.6502E+06	-0.6611E+06
7	0.1087E+07	0.1087E+07	0.1089E+07	0.1094E+07	0.1113E+07
8	-0.1087E+07	-0.1087E+07	-0.1089E+07	-0.1094E+07	-0.1113E+07

(moments) of the internal node are zero. Note that the distortion of the element is quite large in the first and the last distorted mesh layouts.

Next, a uniform line-distributed force is applied along BD in the x_1-direction. The stress field calculated is constant and the same for all mesh layouts. The results are independent of the value of α.

3.2. Deformation of a simply supported beam

In this example, we consider the deformation of a simply supported beam. The geometry and material data of the beam are shown in Fig. 5a. Various mesh layouts shown in Fig. 6 are used to test the behavior of the element. With these mesh layouts, the ratio between the element size and its thickness ranges from 25 to 5. Two load cases are considered. In the first case, a line distributed force is applied at the middle of the beam, see Fig. 5a. In the second case, a line distributed moment is applied at the middle of the beam, see Fig. 5b. The results are plotted in Fig. 7 and Fig. 8, which show good performance of the element. From the figures, it can be seen that even the 2×4 mesh gives good approximations of the deflection of the beam. The results suggest also that the shear locking phenomena are effectively eliminated.

To examine the ability of the element to resist zero energy modes, the beam is now supported and loaded as shown in Fig. 9. The boundary condition and load condition are designed such that zero energy mode associated with translational degrees of freedom may be easily occurred. The beam is modeled by using 2×10 mesh. With a uniformly reduced integration, a typical zero energy mode of the beam is shown in Fig. 10. With the cross reduced integration technique, the

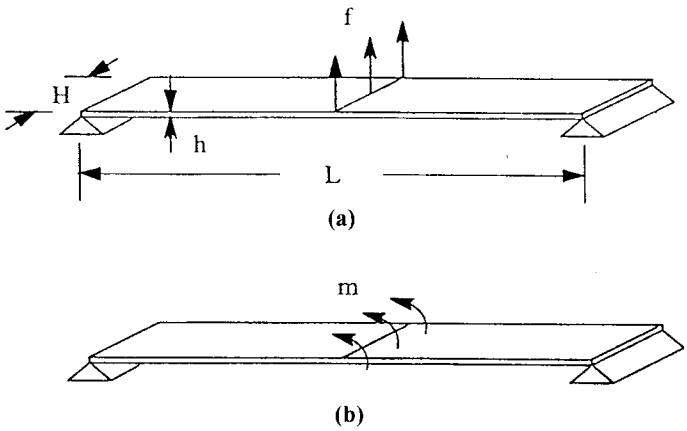

Fig. 5 Deformation of a simply supported beam (Beam length L=1m, width H=0.1m, thickness h=0.01m, Young's modulus E=200Gpa and Poisson's ratio ν=0.3)

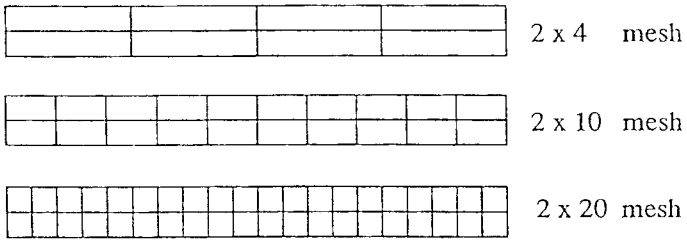

Fig. 6 Deformation of a simply supported beam (Various mesh layouts)

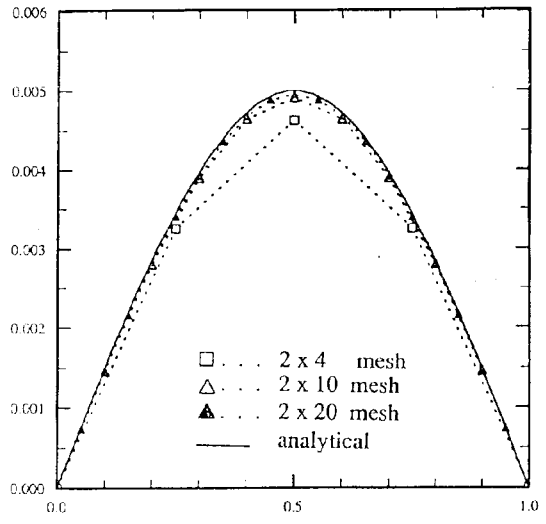

Fig. 7 Deformation of a simply supported beam (Deflection of the beam loaded by the line distributed force)

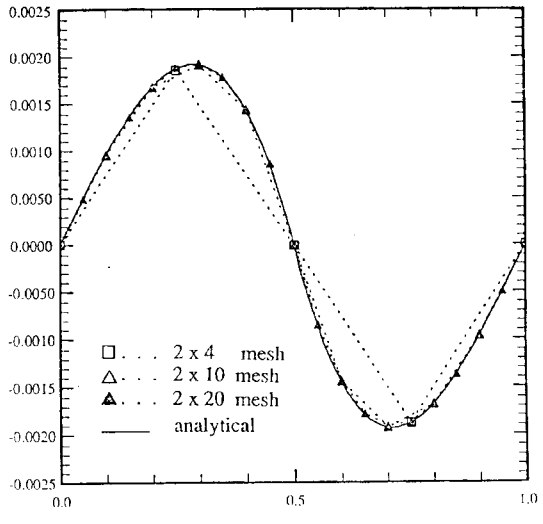

Fig. 8 Deformation of a simply supported beam (Deflection of the beam loaded by the line distributed moment)

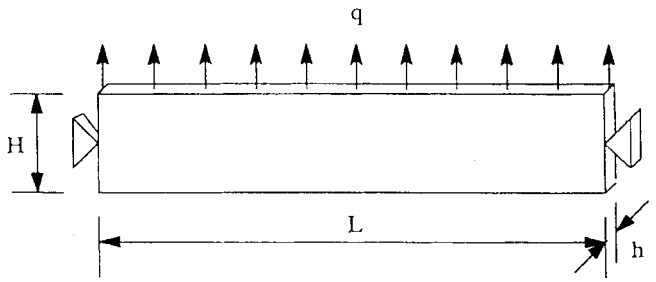

Fig. 9 A simply supported beam loaded by uniformly distributed load

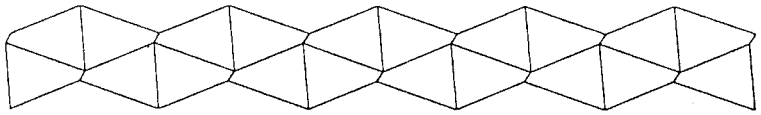

Fig. 10 A typical zero energy mode of the beam

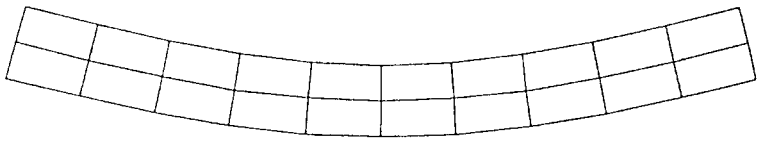

Fig. 11 The correction deformation (scaled) of the beam

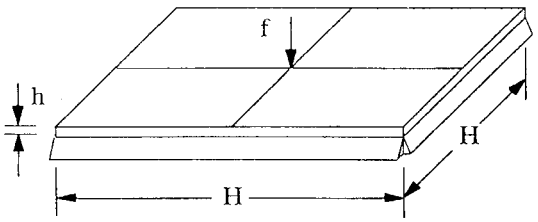

Fig. 12 A simply supported square plate loaded with a concentrate force (Dimension of the plate H=1, thickness h=0.01, Young's modulus $E=2\times10^{11}$ and Poisson's ratio ν=0.3)

deformation of the beam is as shown in Fig. 11, which shows that the zero energy mode has been effectively removed.

3.3. Deformation of a simply supported square plate

In this example, a simple supported square plate subjected to a concentrated force at its center is considered. The problem is depicted in Fig. 12. Three different mesh layouts, i.e., 4×4, 10×10 and 20×20 meshes, are used. Again, the ratio between the element size and its thickness ranges from 25 to 5. The maximum deflection of the plate calculated by using these meshes are plotted in Fig. 13, where the analytical solution is also presented.

To study the effect of the parameter α, the maximum deflection of the plate, simply supported or corner supported, is calculated with a 10×10 mesh and various values for α. The results are shown in Table 3. It can be seen that the solution is not so sensitive to α when α is within the

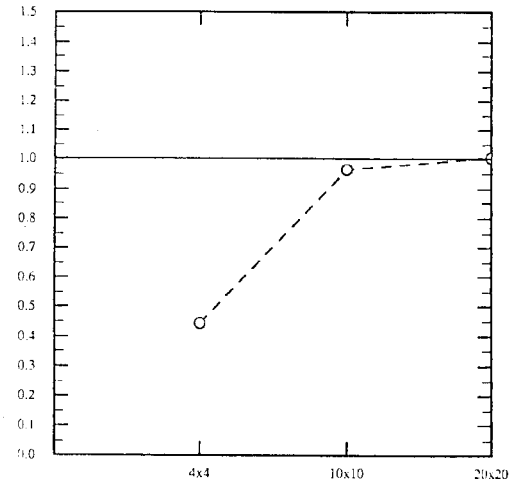

Fig. 13 Maximum deflection of the plate with various mesh layouts

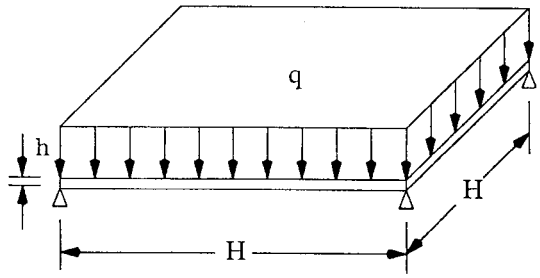

Fig. 14 A corner supported square plate loaded by a uniformly distributed load

Table 3 Deflection of the square plate with different boundary conditions and different values for parameter α

Simply supported		Corner supported	
α	w_{max}	α	w_{max}
0.00001	-0.61662E-02		
0.00010	-0.61654E-02	0000.05	-0.16543E-02
0.00100	-0.61679E-02	0000.10	-0.16533E-02
0.01000	-0.61681E-02	0000.50	-0.16236E-02
0.10000	-0.61156E-02	0001.00	-0.15998E-02
0.20000	-0.59766E-02	0010.00	-0.15581E-02
0.50000	-0.53547E-02	0100.00	-0.15567E-02
1.00000	-0.43534E-02	1000.00	-0.15574E-02
Analytical Zienkiewicz (1977)	-0.63333E-02		-0.15900E-02

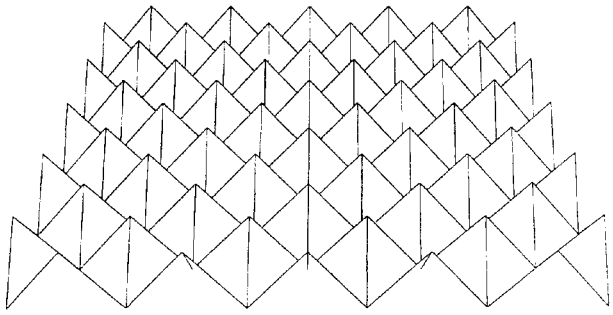

Fig. 15 A corner supported square plate loaded by a uniformly distributed load (Zero energy modes due to a uniformly reduced integration rule)

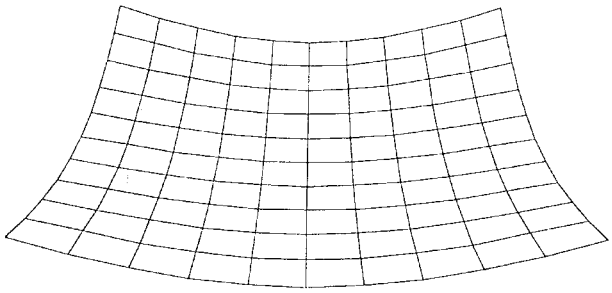

Fig. 16 A corner supported square plate loaded by a uniformly distributed load (Deformation of the plate with the cross reduced integration technique; Displacements are scaled)

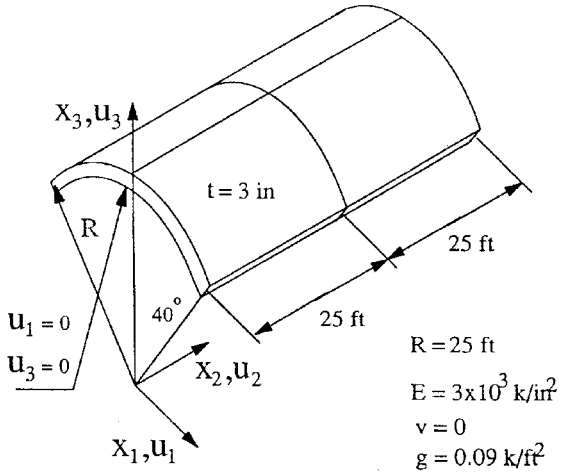

Fig. 17 A curved shell supported by two rigid diaphragms

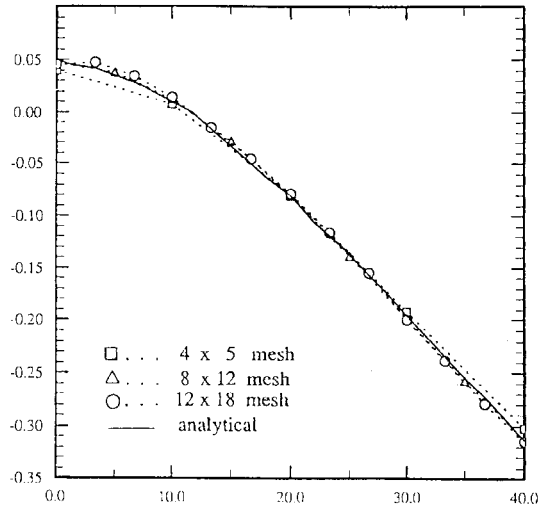

Fig. 18 The vertical displacement of the middle section of the shell

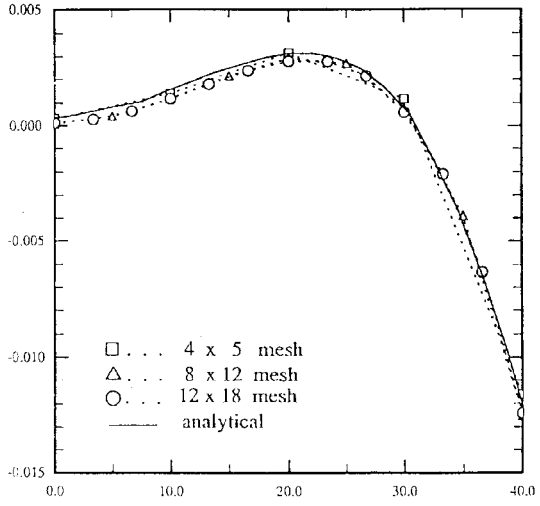

Fig. 19 The displacement in the x_2-direction of the shell at the support

range of 1.02 to 1.20 with both boundary conditions.

Let the plate now be supported at its corners loaded by a uniformly distributed load as shown in Fig. 14. A 10×10 mesh is used to model the plate. With a uniformly reduced integration rule, the deformation mode of the plate is as shown in Fig. 15. The correct deformation mode as shown in Fig. 16 is obtained when the current element is used. The maximum deflection at the central point of the plate is calculated to be 0.00162 with the present element. The analytical maximum deflection of the plate is 0.00159, which is calculated according to $w_{max}=0.0265qL^2/D$ Zienkiewicz (1977). Again, we see that zero energy modes are removed and the locking phenomena are eliminated by using the new reduced integration technique.

3.4. A curved shell supported by rigid diaphragms

Finally, we consider the problem shown in Fig. 17, where a curved shell is supported by two rigid diaphragms and loaded by its own weight. This has been a popular example used to examine the performance of shell elements. Due to double symmetry, only one quarter of the shell needs to be modeled. Three different meshes are used. The vertical displacement in the x_3-direction of the middle section of the shell and the displacement in the x_2-direction at the support are shown in Fig. 18 and Fig. 19, respectively, where the exact solution is obtained by digitizing the curve in Zienkiewicz (1977). The figures show that the shell element with the cross reduced integration technique produces quite good results, even with a relatively coarse mesh (4×5).

4. Conclusions

By decomposing the stiffness of the shell element into two parts and integrating each part with different reduced integration rules, the shell element neither locks nor present any zero energy mode. This same idea can also be implemented in other shell formulations and should also give

similar results. Further research work on this topic is under way and results will be presented in forthcoming papers.

References

Belytschko, T., Tsay, C.S. and Liu, W.K. (1981), "A stabilization matrix for the bilinear mindlin plate element", *Computer Methods in Applied Mechanics and Engineering,* **29**, 313-327.

Belytschko, T. and Tsay, C.S. (1983), "A stabilization procedure for the quadrilateral plate element with one-point quadrature", *Int. J. for Numerical Methods in Engineering,* **19**, 405-419.

Belytschko, T. and Ong, J.S. (1984), "Hourglass control in linear and nonlinear problems", *Computer Methods in Applied Mechanics and Engineering,* **43**, 251-276.

Belytschko, T. and Leviathan, I. (1994), "Physical stabilization of the 4-node shell element with one point quadrature", *Computer Methods in Applied Mechanics and Engineering,* **113**, 321-350.

Cook, R.D. (1981), *Concepts and Applications of Finite Element Analysis*, John Wiley & Sons, Inc. New York.

Hughes, T.J.R. (1987), "Linear static and dynamic finite element analysis", *The Finite Element Method*, Prentice-Hall, Inc.

Jacquotte, O.P. and Oden, J.T. (1983), "Analysis of hourglass instabilities and control in underintegrated finite element methods", *Computer Methods in Applied Mechanics and Engineering,* **19**, 405-419.

Jacquotte, O.P. and Oden, J.T. (1986), "An accurate and efficient control of hourglass instabilities in under-integrated linear and nonlinear elasticity", *Computer Methods in Applied Mechanics and Engineering,* **55**, 105-128.

Liu, W.K., Ong, J.S. and Uras, R.A. (1985), "Finite element stabilization matrices-a unification approach", *Computer Methods in Applied Mechanics and Engineering,* **53**, 13-46.

Noor, A.K., Belytschko, T. and Simo, J.C.(1989), "Analytical and computational models for shells", CED-**3**, *ASME.*

Oldenburg, M. (1988), "Finite element analysis of thin walled structures subjected to impact loading", Doctoral Thesis 1988:69D, Lulea University of Technology, Lulea, Sweden.

Parisch, H. (1995), "A continuum based shell theory for nonlinear applications", *Int. J. for Numerical Methods in Engineering,* **38**, 1855-1883.

Park, K.C., Stanley, G.M. and Flaggs, D.L. (1985), "A uniformly reduced, four-node shell element with consistent rank corrections", *Computers & Structures,* **20**, 129-13.

Pugh, E.D, Hinton, E. and Zienkiewicz, O.C. (1978), "A study of quadrilateral plate bending elements with reduced integration", *Int. J. for Numerical Methods in Engineering,* **12**, 1059-1079.

Vu-Quoc, L. and More, J.A. (1989), "A class of simple and efficient degenerated shell elements-Analysis of global spurious mode filtering", *Computer Methods in Applied Mechanics and Engineering,* **74**, 117-175.

Vu-Quoc, L. (1990), "A perturbation method for dynamic analysis of under-integrated shell elements", *Computer Methods in Applied Mechanics and Engineering,* **79**, 129-172.

Wissmann, J.W., Becker, T. and Moller, H. (1987), "Stabilization of the zero energy modes of under-integrated isoparametric finite elements", *Computational Mechanics,* **2**, 289-306.

Zhong, Z.H. (1991), "A cross reduced integration technique for a bilinear shell element without zero energy modes", *Int. J. Communication of Applied Numerical Methods,* **7**, 569-575.

Zienkiewicz, O.C. (1977), *The Finite Element Method*, Third edition, McGRAW HILL.

Zienkiewicz, O.C., Taylor, R.L. and Too, J.M. (1971), "Reduced integration technique in general analysis of plates and shells", *Int. J. for Numerical Methods in Engineering,* **3**, 275-290.